



Molecular fluctuations inhibit intermittency in compressible turbulence

Ishan Srivastava , Andrew Nonaka, Weiqun Zhang, Alejandro Luis Garcia and John B. Bell

Corresponding author: Ishan Srivastava, isriva@lbl.gov

(Received 20 February 2025; revised 30 September 2025; accepted 5 October 2025)

In the standard picture of fully developed turbulence, highly intermittent hydrodynamic fields are nonlinearly coupled across scales, where local energy cascades from large scales into dissipative vortices and large density gradients. Microscopically, however, constituent fluid molecules are in constant thermal (Brownian) motion, but the role of molecular fluctuations in large-scale turbulence is largely unknown, and with rare exceptions, it has historically been considered irrelevant at scales larger than the molecular mean free path. Recent theoretical and computational investigations have shown that molecular fluctuations can impact energy cascade at Kolmogorov length scales. Here, we show that molecular fluctuations not only modify energy spectrum at wavelengths larger than the Kolmogorov length in compressible turbulence, but also significantly inhibit spatio-temporal intermittency across the entire dissipation range. Using largescale direct numerical simulations of computational fluctuating hydrodynamics, we demonstrate that the extreme intermittency characteristic of turbulence models is replaced by nearly Gaussian statistics in the dissipation range. These results demonstrate that the compressible Navier-Stokes equations should be augmented with molecular fluctuations to accurately predict turbulence statistics across the dissipation range. Our findings have significant consequences for turbulence modelling in applications such as astrophysics, reactive flows and hypersonic aerodynamics, where dissipation-range turbulence is approximated by closure models.

Key words: compressible turbulence, homogeneous turbulence, intermittency

¹Center for Computational Sciences and Engineering, Lawrence Berkeley National Laboratory, 1 Cyclotron Road, Berkeley, CA 94720, USA

²Department of Physics and Astronomy, San Jose State University, 1 Washington Square, San Jose, CA 95192, USA

1. Introduction

A fully developed three-dimensional turbulent state is highly irregular, with energy nonlinearly 'cascading' from large length scales where it is injected to small length scales in an essentially inviscid process, until it is eventually dissipated by the viscosity of the fluid at scales smaller than the dissipation length scale (also known as the Kolmogorov length scale) (Frisch 1995; Eyink & Sreenivasan 2006; Alexakis & Biferale 2018). In incompressible fluids, the energy cascade occurs by a continuous transition of large eddies into smaller and smaller eddies while energy is continually injected at large length scales in a non-equilibrium statistical steady state. Such a cascading phenomenon indicates that the statistical properties of turbulence should be invariant at all scales, as predicted by Kolmogorov's theory of turbulence (Frisch 1995). However, intermittency in turbulent flows result in strong deviations from Kolmogorov's theory at small scales (Frisch & Morf 1981; Paladin & Vulpiani 1987; Frisch 1995; Chevillard, Castaing & Lévêque 2005). Intermittency is characterised by extreme variability of velocities with non-Gaussian, fattailed distributions that appear as localised bursts of extreme vorticity intensification in a largely quiescent flow (Benzi et al. 2008; Yeung, Zhai & Sreenivasan 2015; Wang, Gotoh & Watanabe 2017).

While energy cascades and intermittency have been intensely studied in incompressible fluids, numerous natural and technological phenomena involve turbulent flow of compressible fluids. Important natural applications include astrophysical phenomena such as supernovae, star formation and cosmology (Mac Low & Klessen 2004). Compressible turbulence is also important in technological applications such as high-temperature reactive flows (Hamlington, Poludnenko & Oran 2012), inertial confinement fusion (Bender et al. 2021) and hypersonic vehicle design (Urzay 2018). The dynamics of compressible turbulence is significantly more complicated than incompressible turbulence with nonlinear interactions between solenoidal (shear) and compressive modes of velocity fluctuations along with coupling between the velocity field and thermodynamic fields (pressure and density) (Eyink & Drivas 2018). For example, in addition to dissipative vortices, compressible turbulence is also characterised by the appearance of shock waves (Federrath et al. 2021) and contact surfaces characterised by large density gradients (Benzi et al. 2008). Whereas exact scaling relations for the correlation functions and statistical properties of compressible turbulence have been recently discovered (Wang et al. 2012, 2017; Eyink & Drivas 2018; Donzis & John 2020), further analysis suggests that kinetic energy dissipation occurs due to a distinct mechanism of pressure–work defect (Eyink & Drivas 2018) in addition to local energy cascades (Aluie 2011; Wang et al. 2013). However, despite more complex physical mechanisms, turbulent compressible flows also exhibit local energy cascades, which minimally conserve kinetic energy (Aluie 2011; Wang et al. 2013), and strongly intermittent and variable velocity and thermodynamic fields at smaller length scales (Benzi et al. 2008; Wang et al. 2017; Federrath et al. 2021).

Microscopically, a fluid is a discrete physical system consisting of molecules that are in constant random (i.e. Brownian) motion; an accurate continuum description at small scales requires the use of fluctuating fields. Unlike turbulent fluctuations described above, these molecular fluctuations are thermal in origin, with a covariance structure that is completely described by equilibrium statistical mechanics (Landau & Lifshitz 1980). While thermal fluctuations are present at all scales in a fluid, in non-equilibrium conditions, fluctuations in velocity and thermodynamic fields can become correlated over macroscopic length scales, resulting in interesting macroscale phenomena such as non-equilibrium correlations observed in light scattering (Tremblay, Arai & Siggia 1981), diffusive enhancement by mode coupling (Donev *et al.* 2011), giant fluctuations

(Vailati & Giglio 1997), and hydrodynamic instabilities (Wu, Ahlers & Cannell 1995). It is therefore an important question to ask: at what scales do thermal fluctuations have a significant effect on turbulent fluctuations? While it has been historically accepted that thermal fluctuations do not impact turbulence at scales larger than the mean free path (von Neumann 1949), recent (Bandak et al. 2022) and rediscovered (Betchov 1957) theoretical efforts have remarkably predicted that thermal fluctuations can dominate the kinetic energy spectrum at scales comparable to the dissipative Kolmogorov length scale, which is orders of magnitude larger than the mean free path of most common fluids. These theoretical predictions have been confirmed by very recent modelling efforts (Bell et al. 2022; McMullen et al. 2022), but no experimental confirmation exists. While a recent numerical study on incompressible fluids has discovered that molecular fluctuations replace the extreme-scale intermittency in the far-dissipation range with a Gaussian distribution (Bell et al. 2022), the impact of molecular fluctuations on turbulent intermittency across the whole range of turbulence spectrum remains to be determined. Furthermore, the impact of molecular fluctuations on compressible turbulence has also not been fully explored.

2. Theory and numerical methods

2.1. Fluctuating hydrodynamics theory of compressible fluids

In order to reliably introduce thermal fluctuations in compressible fluid dynamics, we use nonlinear fluctuating hydrodynamics (FHD), originally proposed in the linearised form by Landau & Lifshitz (1959) (see also De Zarate & Sengers 2006). Here, a stochastic flux term is added to the deterministic Navier-Stokes equations, leading formally to a system of stochastic partial differential equations (SPDEs). The stochastic fluxes represent a macroscopic realisation of microscopic degrees of freedom in a thermodynamic system. Specifically, these fluxes are constructed to model fluctuations in hydrodynamic variables that arise from the discrete molecular character of fluids as predicted by statistical mechanics. The linearised form of FHD was justified by Fox & Uhlenbeck (1970a,b), and Bixon & Zwanzig (1969). The nonlinear hydrodynamic fluctuations were later justified by deriving the Fokker-Planck equations of the distribution function of conserved hydrodynamic quantities (Zubarev & Morozov 1983), which then led to the formulation of the associated stochastic differential equations (Español 1998).

The nonlinear FHD equations for a compressible fluid in conservative form are (Srivastava et al. 2023)

$$\frac{\partial}{\partial t}(\rho) = -\nabla \cdot (\rho \mathbf{u}),\tag{2.1a}$$

$$\frac{\partial}{\partial t} (\rho \mathbf{u}) = -\nabla \cdot \left[\rho \mathbf{u} \otimes \mathbf{u} + p \mathbf{I} \right] - \nabla \cdot \left[\mathbf{S} + \widetilde{\mathbf{S}} \right] + \rho \mathbf{a}^F, \tag{2.1b}$$

$$\frac{\partial}{\partial t} (\rho \boldsymbol{u}) = -\nabla \cdot \left[\rho \boldsymbol{u} \otimes \boldsymbol{u} + p \boldsymbol{I} \right] - \nabla \cdot \left[\boldsymbol{S} + \widetilde{\boldsymbol{S}} \right] + \rho \boldsymbol{a}^{F}, \qquad (2.1b)$$

$$\frac{\partial}{\partial t} (\rho E) = -\nabla \cdot \left[\boldsymbol{u} (\rho E + p) \right] - \nabla \cdot \left[\boldsymbol{Q} + \widetilde{\boldsymbol{Q}} \right] - \nabla \cdot \left[\left(\boldsymbol{S} + \widetilde{\boldsymbol{S}} \right) \cdot \boldsymbol{u} \right]$$

$$+ \rho \boldsymbol{a}^{F} \cdot \boldsymbol{u} - \langle \rho \boldsymbol{a}^{F} \cdot \boldsymbol{u} \rangle, \qquad (2.1c)$$

where ρ is the fluid density, \boldsymbol{u} is the velocity, E is the total specific energy, p is the pressure, and I is the identity matrix. The total energy density of the fluid, $\rho E =$ $\rho e + (1/2)\rho(\mathbf{u} \cdot \mathbf{u})$, is the sum of internal energy and kinetic energy, where e is the specific internal energy. In this set of nonlinear FHD equations, the diffusive stress tensor S and heat flux Q are augmented by their stochastic counterparts \widetilde{S} and \widetilde{Q} , respectively. When $\widetilde{S} = \widetilde{Q} = 0$, the FHD equations reduce to the well-known deterministic Navier–Stokes equations for compressible fluids. The term a^F represents a long-wavelength external turbulence acceleration required for maintaining a statistically steady turbulent state. The last term in the energy equation, $-\langle \rho a^F \cdot u \rangle$, represents a thermostat that is used to maintain the system temperature. The details of the diffusive and stochastic fluxes, and the turbulence forcing and thermostat, are presented in the subsections below.

The linearised form of the FHD equations is a well-defined system of SPDEs with equilibrium solutions that are Gaussian random fields with a covariance structure that matches the Gibbs-Boltzmann distribution that is consistent with well-established results in statistical mechanics (Landau & Lifshitz 1980). Although the linearised FHD equations can be rigorously defined with the use of generalised functions, the high irregularity of the stochastic fluxes makes interpreting the fully nonlinear system as SPDEs mathematically ill-defined. To obtain a mathematically tractable model, one needs to introduce a high wavenumber cut-off that is of the order of several mean free paths. In practice, we introduce a cut-off by discretising the system using a finite-volume discretisation with cells that are large enough to have at least $N \ge 50$ molecules per finite-volume cell, resulting in a finite-dimensional system of stochastic differential equations (Srivastava et al. 2023). This system of stochastic differential equations models the effect of thermal fluctuations as measured at the grid scale. Setting $N \ge 50$ ensures that variations in hydrodynamic variables are well-approximated by a Gaussian. The computational methodology used in this work has been demonstrated to accurately capture the effect of thermal fluctuations in both equilibrium and non-equilibrium settings by comparison with theory and molecular gas dynamics simulations (Srivastava et al. 2023). We note that the numerical solution of the FHD equations depends on the specific mesh spacing in the finite-volume discretisation. This reflects the physical property that the variance of fluctuations in hydrodynamic variables depends on the scale at which they are measured.

As such, there is ample numerical evidence that a finite-volume discretisation of the FHD equations accurately models nonlinear hydrodynamics fluctuations in various macroscale non-equilibrium phenomena such as giant fluctuations (Srivastava et al. 2023) and diffusive enhancement (Donev et al. 2011). While FHD has proved remarkably successful for modelling mesoscale laminar flows with thermal fluctuations, matching theory and experiment, numerical solutions of the FHD equations have only very recently been utilised to model turbulence in incompressible fluids with molecular fluctuations (Bell et al. 2022). Here, we consider application of FHD to compressible turbulence. Specifically, we perform direct numerical simulations of homogeneous isotropic turbulence in nitrogen gas at standard temperature and pressure (STP) subjected to a large-wavelength random external solenoidal forcing along with a thermostat to maintain a statistically steady turbulent state. The simulation domain is a periodic cube with sides of length $L \approx 0.2$ mm discretised on a 1024^3 finite-volume grid. The grid size $\Delta x = 1.956 \times 10^{-4}$ mm then sets the small-wavelength (high-wavenumber) cut-off of the numerical solution to the FHD equations that corresponds to the coarse-graining length of the microscopic fluid dynamics. At STP, the mean free path of nitrogen molecules is approximately 70 nm, which is approximately three times smaller than the grid size corresponding to the high-wavenumber cut-off. We also restrict the present study to weakly compressible flows with subsonic turbulent Mach numbers $Ma_t \approx 0.2$ that can exhibit large density variations with contact discontinuities even in the absence of hydrodynamic shocks (Benzi et al. 2008).

2.2. Numerical details

Here, we present the numerical details for solving the nonlinear FHD equations defined in (2.1). For the case of nitrogen gas simulated here, we assume an ideal gas equation of state

$$p = \frac{\rho k_B T}{m},\tag{2.2}$$

where T is the temperature, m is the molecular mass, and k_B is the Boltzmann constant. We assume calorically perfect gas at STP with constant specific heats of a classical diatomic gas. The components of the stress tensor S defined in its Newtonian form are

$$S_{ij} = -\eta \left(\frac{\partial u_i}{\partial x_i} + \frac{\partial u_j}{\partial x_i} \right) - \delta_{ij} \left(\left(\kappa - \frac{2}{3} \eta \right) \nabla \cdot \boldsymbol{u} \right), \tag{2.3}$$

where δ_{ij} is the Kronecker delta, η is the shear viscosity, and κ is the bulk viscosity. The heat flux is $\mathbf{Q} = -\lambda \nabla T$, where λ is the thermal conductivity. The viscosity and thermal conductivity are not treated as constants, but depend on the local state of the fluid (Giovangigli 2012).

The stochastic stress $\tilde{\mathbf{S}}$ is a Gaussian random field with zero ensemble mean, $\langle \tilde{\mathbf{S}} \rangle = 0$, and we use the following efficient form of $\tilde{\mathbf{S}}$, as proposed by Morozov (1984) and Español (1998), in this study:

$$\widetilde{\mathbf{S}}(\mathbf{r},t) = \sqrt{2k_B T \eta} \, \widetilde{\mathcal{Z}} + \left(\sqrt{\frac{k_B \kappa T}{3}} - \frac{\sqrt{2k_B \eta T}}{3} \right) Tr(\widetilde{\mathcal{Z}}) \, \mathbf{I}. \tag{2.4}$$

Here,

$$\widetilde{Z} = \frac{1}{\sqrt{2}} \left(Z + Z^{\mathrm{T}} \right) \tag{2.5}$$

is a symmetric matrix constructed from an uncorrelated Gaussian tensor field $\mathcal Z$ with zero mean and unit variance. The stochastic heat flux $\widetilde{\mathcal Q}$ is

$$\widetilde{\boldsymbol{Q}} = \sqrt{2k_B T^2 \lambda} \, \mathcal{Z}^{(\boldsymbol{Q})},\tag{2.6}$$

where $\mathcal{Z}^{(Q)}$ is an uncorrelated three-dimensional Gaussian vector field with zero mean and unit variance.

A staggered-grid discretisation based on the method-of-lines approach is used to spatially discretise the SPDEs of compressible FHD. Here, the conserved scalar variables, ρ and ρE , and primitive scalar variables, p and T, are discretised at the centre of a finite-volume cell, whereas the vector variables, conserved momentum density ρu and velocity u, are discretised on the normal faces of the grid (Srivastava et~al.~2023). The resulting stochastic ordinary differential equations are integrated explicitly in time using a low-storage third-order Runge–Kutta integrator (Donev et~al.~2010; Srivastava et~al.~2023). The staggered-grid numerical method discretely preserves the fluctuation–dissipation balance (Usabiaga et~al.~2012), which has been confirmed by a correct reproduction of the structure factors of hydrodynamic variables at thermodynamic equilibrium (Srivastava et~al.~2023).

We emphasise here that even though the nonlinear FHD equations and the deterministic Navier–Stokes equations for compressible fluids appear similar, with the exception of the stochastic forcing, they are conceptually completely different in their representation of the underlying hydrodynamic phenomena. The FHD represents a coarse-graining of the molecular description of a fluid, with an underlying assumption that the coarse-graining region has a sufficient number of molecules. The hydrodynamic and thermodynamic fields resulting from the coarse-graining have statistical properties that depend on the scale at

which they are measured, and which become increasingly irregular at smaller scales. This scale dependence is not an artefact, but rather a consequence of the molecular character of the fluid. For computational purposes, a numerical cut-off is introduced that is at least as large as the scale needed to justify the coarse-graining process (Español *et al.* 2009). In the present method, this numerical cut-off is given by the mesh size of the finite-volume discretisation that effectively acts as a low-pass filter for the coarse-grained molecular fluctuations (Eyink 2024), and the accuracy of the FHD description is assessed by renormalisation group invariance of the model to this cut-off (Forster, Nelson & Stephen 1977). In this regard, the invariance of the FHD model to renormalisation group transformation is conceptually different to the traditional numerical convergence of the solution of deterministic Navier–Stokes equations to an underlying continuum model.

2.3. Turbulence forcing and thermostat

A statistically steady homogeneous isotropic turbulent state is achieved by forcing the system with a stochastic process using the formulation of Eswaran & Pope (1988). An external force $\rho a^F(r,t)$ corresponding to a long-wavelength acceleration $a^F(r,t)$ is added to the momentum equation to drive turbulence. The forcing is applied only on wavevectors k whose wavenumbers lie inside the spherical shell of radius $2\sqrt{2} k_0$, such that $|k| \le 2\sqrt{2} k_0$, where $k_0 = 2\pi/L$.

Mathematically, consider an Ornstein-Uhlenbeck process for a complex-valued vector $\boldsymbol{b}(\boldsymbol{n},t)$ as

$$db(n) = Ab(n) dt + BdW, (2.7)$$

where $\mathbf{n} = (n_x, n_y, n_z)$ are integer indices such that $1 \le |\mathbf{n}| \le 2\sqrt{2}$ limits the forcing to long wavelengths, and \mathbf{W} is a vector of complex Wiener processes. The matrices in the Ornstein-Uhlenbeck process are

$$\mathbf{A} = \frac{1}{T_L} \mathbf{I}, \quad \mathbf{B} = \sigma \sqrt{\frac{1}{T_L}} \mathbf{I}, \tag{2.8}$$

where *I* is the identity matrix. Therefore, we have (Gardiner 1985)

$$\langle \boldsymbol{b}(\boldsymbol{n},t) \cdot \boldsymbol{b}^*(\boldsymbol{n}',t+s) \rangle = \frac{\sigma^2}{2} e^{-s/T_L} \, \delta_{\boldsymbol{n},\boldsymbol{n}'}, \tag{2.9}$$

where σ and T_L control the amplitude and time scale of external forcing. In compressible turbulence, both solenoidal and dilatational modes can be forced independently; in this study, we focus on solenoidal forcing only. To do so, we apply a projection operator P on b(n, t) such that $\tilde{b}(n, t) = P \cdot b(n, t)$ is projected onto a plane normal to $k = 2\pi n/L$, where

$$P = \left(I - \frac{kk^{\mathrm{T}}}{|k|^2}\right). \tag{2.10}$$

The real-space turbulence forcing is then formulated as

$$\boldsymbol{a}^{F}(\boldsymbol{r},t) = \operatorname{Re}\left[\sum_{1 \leq |\boldsymbol{n}| \leq 2\sqrt{2}} \left(\tilde{\boldsymbol{b}}(\boldsymbol{n}) + \tilde{\boldsymbol{b}}^{*}(-\boldsymbol{n})\right) e^{i\boldsymbol{k}\cdot\boldsymbol{r}}\right]. \tag{2.11}$$

The external turbulence forcing adds energy to the compressible fluid that dissipates as heat, causing an increase in the system temperature. To maintain a statistically steady state,

energy is continually removed from the system using a sink. At each time step, we compute the mean power due to the external forcing as $\langle \rho(r) \, a^F(r) \cdot u(r) \rangle$, which is uniformly removed as a sink term in the energy equation. We note that at thermodynamic equilibrium without forcing in FHD simulations, no sink is needed because the fluctuation–dissipation balance ensures a statistically steady state.

2.4. Simulation details and statistics

We ran simulations with the initial state of nitrogen gas at STP conditions of density $\rho_0 = 1.13 \times 10^{-3} \text{ g cm}^{-3}$ and T = 300 K, where the mean free path of nitrogen molecules is approximately 70 nm. A fully periodic system with $L = 2.0032 \times 10^{-2}$ cm was initialised. Massively parallel simulations on a 1024³ finite-volume grid were conducted for both deterministic Navier-Stokes and FHD on high-performance computing platforms (see the Appendix for details). The finite-volume grid spacing $\Delta x = 1.956 \times 10^{-4}$ mm corresponds to $N \approx 1.8 \times 10^5$ molecules of nitrogen per finite-volume cell. The time step of the simulation was fixed at $\Delta t = 1.25 \times 10^{-11}$ s in both deterministic Navier-Stokes and FHD simulations. The thermodynamic and transport properties of the gas were modelled with a hard-sphere approximation based on the prescription by Giovangigli (2012). A turbulent solenoidal forcing corresponding to $\sigma = 6 \times 10^9 \,\mathrm{cm \, s^{-2}}$ and $T_L =$ 1.5×10^{-4} s was applied at the start to both deterministic Navier-Stokes and FHD simulations. In each case, the simulations were first run for approximately 1.125×10^6 time steps until they reached a statistical steady state. Thereafter, the simluations were run for at least longer than $8\tau_{\lambda}$, where τ_{λ} is the eddy turnover time during which the statistics were collected.

3. Results

3.1. Dissipation-range turbulence with molecular fluctuations

We first probe dissipation-range intermittency by analysing the probability density function (PDF) of local vorticity obtained from direct numerical simulations (see § I of the supplementary material is available at https://doi.org/10.1017/jfm.2025.10796 for details on the numerical computation of local vorticity) averaged over at least $8\tau_{\lambda}$, where τ_{λ} is the eddy turnover time. Intermittency in turbulent flows results in extreme bursts of local vorticity that are spatially interspersed within regions of relatively quiescent flow; as a result, the statistics of vorticity become highly non-Gaussian (Frisch 1995). This is confirmed in figure 1(a), which shows non-Gaussian tails in the PDF of the vector components of local vorticity ω normalised by the ensemble standard deviation σ_{ω} . Remarkably, when molecular fluctuations are included (labelled FHD), a more Gaussianlike PDF is obtained that indicates the homogenising effect of molecular fluctuations at dissipation scales that are approximately three times larger than the molecular mean free path. In FHD simulations at thermodynamic equilibrium in the absence of external turbulent forcing, the PDF is completely Gaussian. For this case, the ensemble standard deviation of local vorticity σ_{ω}^{eq} matches well with theoretical predictions of equilibrium thermodynamics (Landau & Lifshitz 1980), to within less than 1 %. The homogenising effect of molecular fluctuations is readily observed in the visualisation of local vorticity magnitude $|\omega|$ normalised by σ_{ω}^{eq} in figures 1(b) and 1(c). Whereas in deterministic simulations, regions of high vorticity are highly localised around large regions of quiescence, FHD simulations exhibit a more diffuse distribution of vorticity. Here, localised regions of high vorticity are overlaid on homogeneously distributed fluctuating velocity (and vorticity) as a result of thermal equipartition from molecular fluctuations.

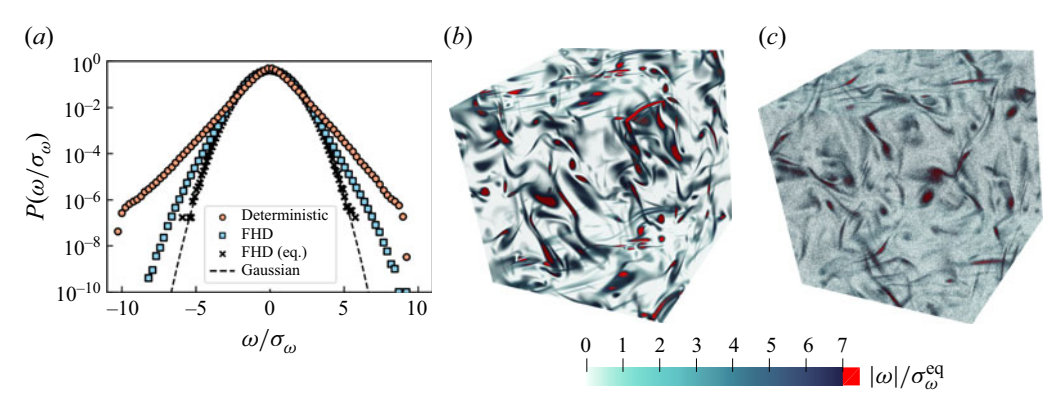


Figure 1. (a) The PDFs of local vorticity ω normalised by their ensemble standard deviation σ_{ω} averaged over at least $8\tau_{\lambda}$, where τ_{λ} is the eddy turnover time for deterministic and FHD simulations. The PDF from an FHD simulation at thermodynamic equilibrium without turbulent forcing, FHD (eq.), is also plotted. Three-dimensional visualisations of local vorticity magnitude $|\omega|$ in (b) deterministic and (c) FHD simulations. Here, $|\omega|$ is normalised by the standard deviation of vorticity fluctuations at thermodynamic equilibrium $\sigma_{\omega}^{eq} \approx 5 \times 10^6 \text{ s}^{-1}$; the standard deviations of vorticity fluctuations are $\sigma_{\omega} \approx 7.3 \times 10^6 \text{ s}^{-1}$ and $\sigma_{\omega} \approx 6.3 \times 10^6 \text{ s}^{-1}$ for deterministic and FHD simulations, respectively.

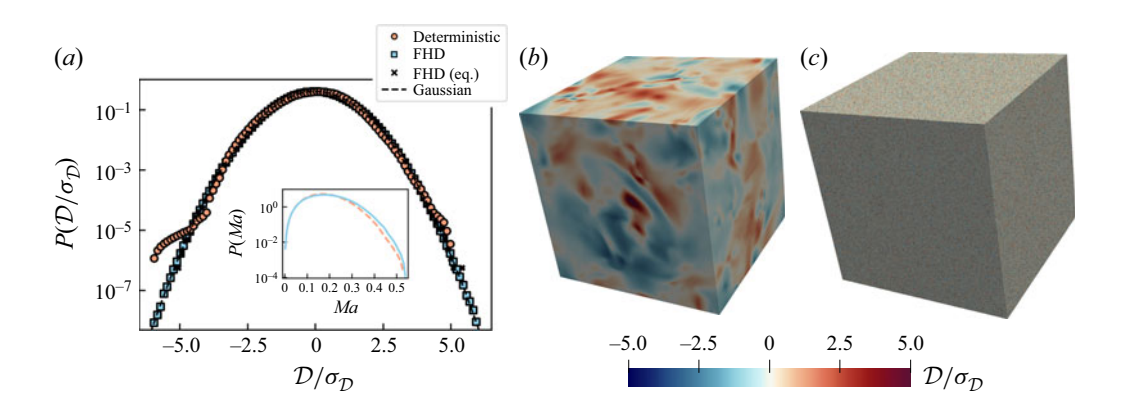


Figure 2. (a) The PDF of local divergence \mathcal{D} normalised by its ensemble standard deviation $\sigma_{\mathcal{D}}$ for deterministic and FHD simulations. The inset shows the PDF of local Mach number Ma in FHD (orange) and deterministic (blue) simulations. Three-dimensional visualisations of local divergence in (b) deterministic and (c) FHD simulations. Here, \mathcal{D} is normalised by the standard deviation of divergence fluctuations that are $\sigma_{\mathcal{D}} \approx 3.1 \times 10^5 \, \mathrm{s}^{-1}$ and $\sigma_{\mathcal{D}} \approx 8.7 \times 10^6 \, \mathrm{s}^{-1}$ for deterministic and FHD simulations, respectively.

In FHD simulations at thermodynamic equilibrium, the local vorticity is a completely Gaussian random field (see figure S1 of the supplementary material).

Compressible turbulence exhibits strong hydrodynamic shocks (Federrath *et al.* 2021); however, even weakly compressible subsonic compressible turbulent flows can exhibit large density gradients without shocks (Benzi *et al.* 2008). Here, we restrict ourselves to nonlinear subsonic flows without any strong shock effects (Sagaut & Cambon 2018), but where the local Mach numbers can be as high as 0.5 (see inset of figure 2a) such that compressibility effects are not negligible, and we observe regions of large density variations (see figure S2 of the supplementary material for three-dimensional visualisations of local density fields). The dilatational behaviour of turbulence is analysed by the PDF of local divergence $\mathcal{D} = \nabla \cdot \boldsymbol{u}$ normalised by the ensemble standard deviation

 $\sigma_{\mathcal{D}}$ in figure 2(a) (see § I of the supplementary material for details on the numerical computation of local divergence). The PDF is nearly Gaussian for FHD simulations, and is coincident with the fully Gaussian PDF for FHD simulations without turbulent forcing. Deterministic simulations exhibit modest non-Gaussian tails for both positive and negative divergence. Furthermore, the instantaneous PDFs exhibit significant temporal variability in deterministic simulations, whereas the variability is very small for FHD simulations (see figure S3 of the supplementary material for PDFs of local divergence). On average, however, divergence in deterministic simulations is negatively skewed, with skewness $S \approx -0.12 \pm 0.19$, whereas $S \approx 0$ for FHD simulations. More spatial volume is associated with expansion than compression in deterministic simulations (Sagaut & Cambon 2018), whereas FHD simulations exhibit nearly equal volumes of expansion and compression.

The strength of dilatation is much stronger in FHD simulations ($\sigma_D \approx 8.7 \times 10^6 \, \mathrm{s}^{-1}$) compared to deterministic simulations ($\sigma_D \approx 3.1 \times 10^5 \, \mathrm{s}^{-1}$). Molecular fluctuations in FHD simulations excite both vortical and dilatational modes of fluid motion via equipartition, whereas dilatational modes are indirectly excited through nonlinear coupling with the fluid vorticity in deterministic simulations (Sagaut & Cambon 2018), which is a much weaker effect for pure solenoidally forced turbulent flows considered here. In FHD simulations with no turbulent forcing, $\sigma_D^{eq} \approx 8.6 \times 10^6 \, \mathrm{s}^{-1}$, which is nearly equal to its value in FHD simulations with turbulent forcing, thus demonstrating that molecular fluctuations completely dominate the dilatational dynamics. The differences are apparent in figures 2(b) and 2(c), which visualise local \mathcal{D}/σ_D fields. While deterministic simulations exhibit extended regions of both positive and negative divergence separated by contact discontinuities, the local divergence field is spatially nearly Gaussian in FHD simulations.

Here, we remark that in order to derive various hydrodynamic quantities, such as vorticity and divergence discussed above, we computed the numerical derivatives of the velocity field on the finite-volume grid. We emphasise that the discrete numerical operators that are used to derive these quantities are the same operators that were used to evaluate derivatives in the numerical solution algorithm for the FHD equations, thus making them consistent with the underlying numerical algorithm. As with the numerical solution of the FHD equations, the derived hydrodynamic quantities also depend on the mesh resolution; however, this resolution dependence is physically correct since the variance of thermal fluctuations depends on the scale of measurement.

3.2. Turbulence and thermal dissipation: separation of scales

In order to provide an objective comparison between deterministic Navier–Stokes and FHD simulations, we compute various microscale and dissipation (Kolmogorov) scale turbulence quantities from the simulations. Unlike deterministic Navier–Stokes equations, the computation of velocity gradients in FHD is highly scale-dependent, and as such, they do not represent an objective physical quantity. Therefore, any derived microscale and dissipation scale turbulence quantities from local velocity gradients will depend on the low-pass filter cut-off for the hydrodynamic and thermodynamic fields. In order to define an objective and meaningful turbulent energy dissipation rate, we compute the mean low-pass filtered enstrophy $\langle \Omega^{<}(k) \rangle$ from the kinetic energy spectrum $\langle E(k) \rangle = (1/2) \langle \hat{u}(k) \cdot \hat{u}(k)^* \rangle$ as

$$\langle \Omega^{<}(k) \rangle = \int_{0}^{k} q^{2} \langle E(q) \rangle \, \mathrm{d}q,$$
 (3.1)

where $\hat{u}(k)$ is the total velocity in the Fourier space. Subsequently, a mean low-pass filtered dissipation rate is computed as $\langle \epsilon^{<}(k) \rangle = (2\langle \eta \rangle/\langle \rho \rangle) \, \Omega^{<}(k)$. Figure 3 shows $\langle \epsilon^{<}(k) \rangle$

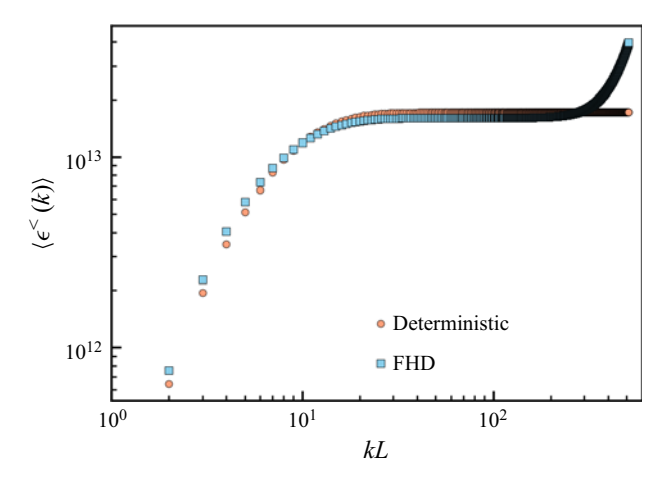


Figure 3. Mean low-pass filtered dissipation rate $\langle \epsilon^{<}(k) \rangle$ as a function of the wavenumber k computed from the mean mean low-pass filtered enstrophy in (3.1) for deterministic Navier–Stokes and FHD simulations of compressible turbulence.

as a function of the filtering wavenumber for deterministic Navier–Stokes and FHD simulations. At large cut-off wavenumbers, $\langle \epsilon^<(k) \rangle$ plateaus to a constant value owing to very small velocities at small scales, whereas in FHD simulations, $\langle \epsilon^<(k) \rangle$ plateaus to a nearly similar constant value before rapidly increasing at even higher wavenumbers. This increase is attributed to dissipation primarily occurring from molecular fluctuations at small scales, which is an effect distinct from turbulent eddy fluctuations (Eyink & Jafari 2022). As such, the plateau value of $\langle \epsilon^<(k) \rangle$, hereby denoted $\langle \epsilon^< \rangle$, provides a physically meaningful and objective definition of turbulent energy dissipation rate in deterministic Navier–Stokes and FHD simulations. Furthermore, the current experimental techniques for turbulence measure coarse-grained fluid velocities and dissipation rates at scales much larger than the Kolmogorov scale, and as such, are consistent with the low-pass filtered definition of these quantities. Future experiments that can measure sub-Kolmogorov-scale velocities can potentially disentangle dissipation due to molecular fluctuations from turbulence dissipation (Bandak *et al.* 2022).

Using the prescription for low-pass filtered turbulent energy dissipation rate discussed above, we derived various microscale and dissipation-scale quantities from the simulations. In particular, we computed the following microscale quantities: (i) turbulent Mach number $Ma_t = u'/\langle c \rangle$, where c is the local speed of sound and u' is the root mean square velocity that is computed from the kinetic energy spectrum as

$$u'^{2} = \frac{2}{3} \int_{0}^{\infty} \langle E(k) \rangle \, \mathrm{d}k; \tag{3.2}$$

(ii) microscale Reynolds number $Re_{\lambda} = \langle \rho \rangle u' l_{\lambda} / \langle \eta \rangle$ corresponding to the Taylor microscale length (Pope 2001)

$$l_{\lambda} = \sqrt{\frac{2u^{2}}{\left(\left(\frac{\partial u_{1}}{\partial x_{1}}\right)^{2}\right)}},\tag{3.3}$$

where $\langle (\partial u_1/\partial x_1)^2 \rangle = (2/9)\langle \Omega^{<} \rangle$ assuming isotropy of flow. Per the discussion above, we use the plateau value of $\langle \Omega^{<} \rangle$ to estimate the velocity gradients. A microscale eddy

Case	Ma_t	Re_{λ}	$l_{\lambda} \times 10^{-3} \text{ (cm)}$	$\tau_{\lambda} \times 10^{-7} \text{ (s)}$	$l_{\eta} \times 10^{-4} \text{ (cm)}$	$\tau_{\eta} \times 10^{-7} \text{ (s)}$
D-NS	0.20	34.9	1.53	4.13	1.28	1.01
FHD	0.21	40.1	1.67	4.27	1.26	0.97

Table 1. Mean turbulence statistics obtained from the simulations. Here, D-NS denotes deterministic Navier–Stokes, Ma_t is the turbulent Mach number, Re_{λ} is the microscale Reynolds number, l_{λ} is the Taylor microscale length, τ_{λ} is the eddy turnover time, l_{η} is the Kolmogorov length corresponding to the total dissipation rate, and τ_{η} is the Kolmogorov time scale.

turnover time is also computed as $\tau_{\lambda} = l_{\lambda}/u'$. To compute dissipation-scale quantities, we use the plateau value of mean low-pass filtered dissipation rate $\langle \epsilon^{<} \rangle$ as described above. The dissipation (Kolmogorov) length scale is calculated as $l_{\eta} = (\langle \eta \rangle^3/\langle \rho \rangle^3 \langle \epsilon^{<} \rangle)^{1/4}$, and the corresponding Kolmogorov (small eddy turnover) time scale is calculated as $\tau_{\eta} = (\langle \eta \rangle/\langle \rho \rangle \langle \epsilon^{<} \rangle)^{1/2}$.

Table 1 lists the microscale and dissipation-scale turbulence statistics for deterministic Navier–Stokes and FHD simluations. By using a low-pass filter for velocity gradients and dissipation rates in the Fourier space as described above, we obtain a meaningful comparison between the two simulations. We note that in the case of deterministic simulation, the turbulent Mach number Re_{λ} computed above matches reasonably well with its value $Re_{\lambda} = 41.8$ computed directly from the velocities in the real space on the finite-volume grid. The small discrepancy between the two values is possibly attributed to complex enstrophy budgeting among the nonlinearly coupled dilatational and solenoidal components of the turbulence velocity.

3.3. Thermal energy crossover scale in the energy spectrum

We now discuss the length scales at which molecular fluctuations have an appreciable influence on compressible turbulence beyond the dissipation scale. The total energy spectra $E(k) = (1/2)\langle \hat{\boldsymbol{u}}(k) \cdot \hat{\boldsymbol{u}}(k)^* \rangle$ of a turbulent flow can be approximately divided into the following three regimes (see figure 4a). (i) The far-dissipation range (FDR) represents the smallest length scales, specifically wavenumbers larger than the Kolmogorov wavenumber $k_n = v^{-3/4} \langle \epsilon \rangle^{1/4}$, where ν is the kinematic viscosity, and $\langle \epsilon \rangle$ is the total mean dissipation rate. This regime is dominated by viscous dissipation and strong intermittency (Kraichnan 1967), and molecular fluctuations strongly dominate turbulence at these length scales, as shown above. (ii) The inertial sub-range (ISR) represents length scales where energy cascades from larger eddies to smaller eddies in a scale-invariant manner, and energy spectra have the form $E(k) \propto \langle \epsilon \rangle^{2/3} k^{-5/3}$ (Frisch 1995). (iii) The near-dissipation range (NDR) (Frisch & Vergassola 1991; Buaria & Sreenivasan 2020) that extends approximately from $k_n/30$ to k_n represents the transition between ISR and FDR where the viscous effects start to become important and intermittency starts growing rapidly (Chevillard *et al.* 2005). Here, the turbulent spectra drop exponentially as $E(k) = u_{\eta}^2 l_{\eta} \exp(-\beta k l_{\eta})$, where $u_{\eta} = (\langle \epsilon \rangle \nu)^{1/4}$ is the Kolmogorov velocity scale, $l_{\eta} = (\nu^3/\langle \epsilon \rangle)^{1/4}$ is the Kolmogorov length, and β is the rate of exponential decay of the spectrum that typically ranges from 3 to 7 (we have fixed $\beta = 5$ in our analysis) (Khurshid, Donzis & Sreenivasan 2018).

Molecular fluctuations introduce another length scale in the turbulence spectrum (Bandak *et al.* 2021). From equilibrium thermodynamics, the contribution of molecular

I. Srivastava, A. Nonaka, W. Zhang, A.L. Garcia and J.B. Bell

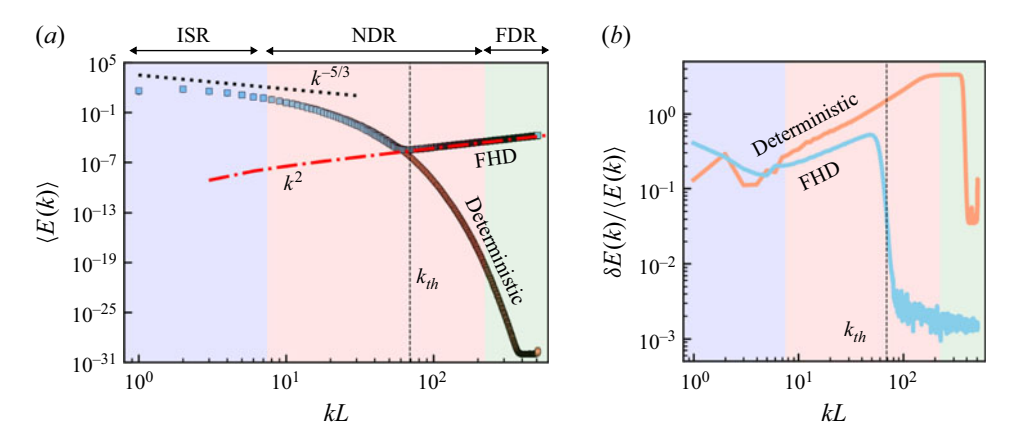


Figure 4. (a) Comparison of the total kinetic energy spectrum $\langle E(k) \rangle$ in FHD versus deterministic simulations. Three approximate ranges of length scales are highlighted: inertial sub-range (ISR, in blue), near-dissipation range (NDR, in pink) and far-dissipation range (FDR, in green). In FHD simulations the thermal spectrum $E_{th}(k) = (3k_B \langle T \rangle/2\langle \rho \rangle)4\pi k^2$ (red dash-dotted line) dominates for wavenumbers larger than the thermal crossover scale k_{th} , where k_B is the Boltzmann constant. (b) Standard deviation in total kinetic energy spectrum $\delta E(k) = \langle (E(k) - \langle E(k) \rangle)^2 \rangle^{1/2}$ normalised by $\langle E(k) \rangle$.

fluctuations to the energy spectrum (assuming no net flow, i.e. $\langle u \rangle = 0$) is

$$E_{th}(k) = \frac{3k_B \langle T \rangle}{2\langle \rho \rangle} 4\pi k^2, \tag{3.4}$$

which is 'equipartitioned' white noise with variance $3k_B\langle T\rangle/2\langle \rho\rangle$ at all scales. The wavenumber k_{th} at which molecular fluctuations are approximately equal in magnitude to the turbulent spectrum is (Bandak *et al.* 2021)

$$u_{\eta}^2 l_{\eta} \exp\left(-\beta k_{th} l_{\eta}\right) \approx \frac{k_B \langle T \rangle}{\langle \rho \rangle} k_{th}^2.$$
 (3.5)

Indeed, in figure 4(a), we observe that for FHD simulations, the total energy spectrum crosses over from an exponential decay in the NDR to being dominated by the thermal spectrum $E_{th}(k)$ at high wavenumbers. The agreement with $E_{th}(k)$ is remarkable without any fitting parameters. The thermal crossover wavenumber k_{th} is approximately three times smaller than the Kolmogorov wavenumber k_{η} , and its predicted value from (3.5) (shown by the dashed vertical black line) matches well with the observed crossover to $E_{th}(k)$ (shown by the dash-dotted red line). While the ratio k_{th}/k_{η} depends on turbulence conditions, such as density, viscosity, temperature and mean dissipation rate (Bandak *et al.* 2022; Bell *et al.* 2022), the relationship between k_{th} and k_{η} is fairly robust, and varies only very marginally across a wide range of turbulence conditions (Bell *et al.* 2022).

The crossover into the thermal regime is also observed for the dilatational part of the energy spectrum $E_d(k) = (1/2)\langle \hat{\boldsymbol{u}}_d(k) \cdot \hat{\boldsymbol{u}}_d(k)^* \rangle$, as shown in figure 5(a), where $\hat{\boldsymbol{u}}_d$ is the dilatational (curl-free) part of the total velocity $\hat{\boldsymbol{u}}$. At low wavenumbers, the total kinetic energy is dominated by solenoidal modes since the external turbulence forcing is solenoidal (see figure S4 of the supplementary material for $\langle E_d(k)/E(k)\rangle$). However, following a rapid decay in the NDR, $E_d(k)$ crosses over to $E_{d,th}(k) = (1/3) E_{th}(k)$ at the wavenumber k_{th} in FHD simulations. The factor 1/3 appears because one-third of the thermal energy of molecular fluctuations is 'equipartitioned' into the dilatational part, and two-thirds into the solenoidal part of the total kinetic energy.

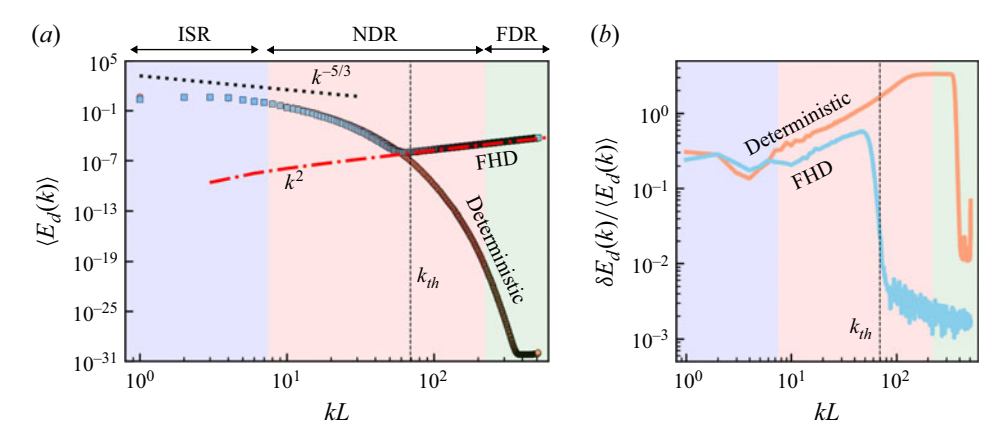


Figure 5. (a) Comparison of dilatational kinetic energy $\langle E_d(k) \rangle$ in FHD versus deterministic simulations. The FHD simulations transition over to the thermal energy spectrum is $E_{d,th}(k) = (1/3) E_{th}(k)$ (red dash-dotted line) at k_{th} . (b) Standard deviation in the dilatational kinetic energy spectrum $\delta E_d(k) = \langle (E_d(k) - \langle E_d(k) \rangle)^2 \rangle^{1/2}$ normalised by $\langle E_d(k) \rangle$.

The picture that emerges from these observations is that the impact of molecular fluctuations on turbulence is not limited to dissipation scales in the FDR, but appears at larger thermal crossover scales in the NDR. While the simulations in this study have been conducted at low Reynolds numbers due to computational constraints, we can estimate the scales at which molecular fluctuations will be significant in several practical scenarios. For example, following Garratt (1994) and Bandak *et al.* (2021), in an atmospheric boundary layer assumed to be composed entirely of nitrogen at $T = 300 \, \text{K}$, the energy dissipation rate is $\epsilon = 400 \, \text{cm}^2 \, \text{s}^{-3}$, kinematic viscosity of nitrogen is $\nu = 0.16 \, \text{cm}^2 \, \text{s}^{-1}$, and density is $\rho = 1.1 \times 10^{-3} \, \text{g cm}^{-3}$. The mean free path is $l_{mfp} \approx 70 \, \text{nm}$, while the Kolmogorov length scale is $l_{\eta} = 0.57 \, \text{mm}$. From (3.2), the thermal crossover length scale at which molecular fluctuations will dominate is $l_{th} \approx 1.3 \, \text{mm}$, which is over four orders of magnitude larger than the mean free path.

3.4. Molecular fluctuations impact turbulence statistics across the near-dissipation range It is apparent that mean turbulence properties are significantly modified in the NDR at all length scales smaller than $1/k_{th}$. However, it is well known that intermittency in turbulence starts building up in the ISR, and rapidly increases in the NDR, where viscous effects start to intensify (Frisch & Vergassola 1991; Chevillard *et al.* 2005). Therefore, even though molecular fluctuations do not affect the ensemble-averaged turbulence properties such as the energy spectrum $\langle E(k) \rangle$ for $k < k_{th}$, we can expect them to modify the statistical properties of turbulence.

Indeed, a remarkable picture emerges where the large temporal statistical variability of turbulence in the NDR is significantly reduced due to molecular fluctuations. Figures 4(b) and 5(b) respectively show the standard deviation of the total energy $\delta E(k)$ and dilatational energy spectra $\delta E_d(k)$ normalised by the mean value averaged over at least $8\tau_{\lambda}$. The growth of $\delta E(k)$ and $\delta E_d(k)$ is much slower in FHD than in deterministic simulations for $k < k_{th}$, thus implying increased statistical stability of the dynamical turbulent system with molecular fluctuations. For $k > k_{th}$, the statistical variability plummets by two orders of magnitude in FHD simulations, whereas it keeps increasing with k for deterministic simulations up to the beginning of the FDR. The eventual drop-off in $\delta E(k)$ and $\delta E_d(k)$ at very high k results from limitations in numerical precision.

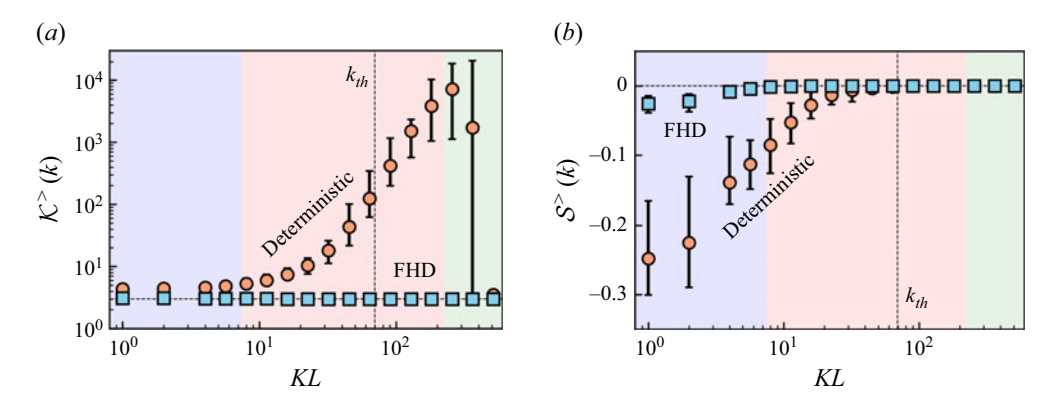


Figure 6. (a) Filtered kurtosis (flatness) $K^>(k)$ and (b) filtered skewness $S^>(k)$ of the velocity gradient $\partial_x u^>$, where $u^>$ is the high-pass filtered velocity obtained by zeroing out all the Fourier modes for wavenumbers lesser than k in the velocity field. The horizontal dashed line corresponds to the kurtosis and skewness of a Gaussian random field with $K^>=3$ and $S^>=0$ for all wavenumbers. The error bars denote the ensemble standard deviation.

Next, we quantify scale-dependent spatial intermittency of turbulence through high-pass filtered skewness $S^{>}(k)$ and kurtosis (flatness) $K^{>}(k)$ of the velocity gradient $\partial_x u^{>}$ that are computed as

$$S^{>}(k_i) = \frac{\overline{(\partial_x \mathbf{u}^{>})^3}}{\left[\overline{(\partial_x \mathbf{u}^{>})^2}\right]^{3/2}}, \quad \mathcal{K}^{>}(k_i) = \frac{\overline{(\partial_x \mathbf{u}^{>})^4}}{\left[\overline{(\partial_x \mathbf{u}^{>})^2}\right]^2}, \tag{3.6}$$

where

$$\overline{(\partial_x \boldsymbol{u}^{>})^n} = \frac{1}{V} \int d\boldsymbol{r} \left(\partial_x \boldsymbol{u}^{>}(\boldsymbol{r})\right)^n, \tag{3.7}$$

and $u^>$ is the high-pass filtered velocity. Numerically, $u^>$ is obtained by first computing the discrete Fourier transform of the velocity field over the finite-volume grid and zeroing out the Fourier modes for wavenumbers smaller than k, followed by a discrete inverse Fourier transform to obtain the high-pass filtered velocity on the same finite-volume grid. Once $u^>$ is obtained, $S^>(k)$ and $K^>(k)$ are calculated by numerically computing the derivative $\partial_x u^>$ using the same gradient operators as employed in the numerical simluation of the FHD equations.

In an intermittent dynamical system, $K^>(k)$ is expected to grow unboundedly with k in the NDR and into the FDR as regions of intense turbulent activity become increasingly localised in smaller fractions of the system volume (Frisch 1995). A negative skewness for a turbulent system implies energy cascade from large to small scales (Frisch 1995), and its magnitude ranges from $S \approx -0.5$ to $S \approx -0.3$. In a fully Gaussian distribution, S = 0 and K = 3.

In the present simulations, rapidly increasing intermittency from its build up in the ISR and propagation through the NDR and into the FDR is observed in the deterministic case, as seen by the variation of $\mathcal{K}^>$ in figure 6(a). In a remarkable contrast, $\mathcal{K}^>(k) \approx 3$ at all wavenumbers in FHD simulations, thus demonstrating that the intermittent dynamics is completely inhibited not just in the FDR, but well into the NDR. Furthermore, large variations in $\mathcal{K}^>(k)$ in deterministic simulations at high k, which are indicative

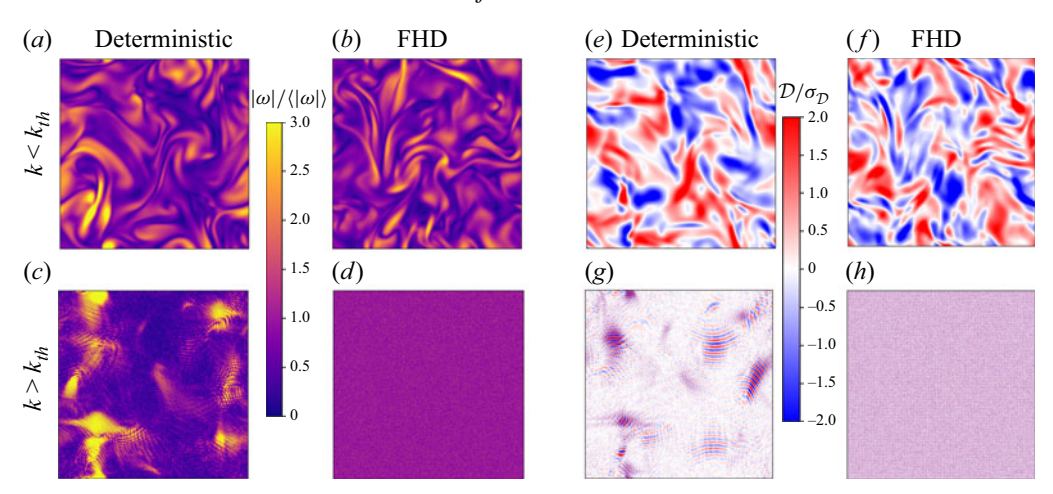


Figure 7. Cross-sectional visualisations of the local vorticity magnitude $|\omega|$ (normalised by the ensemble mean $\langle |\omega| \rangle$) only for wavenumbers $k < k_{th}$ in (a) deterministic and (b) FHD simulations. (c,d) Same as (a,b), respectively, but only for wavenumbers $k > k_{th}$. Cross-sectional visualisation of the local divergence \mathcal{D} (normalised by the ensemble standard deviation $\sigma_{\mathcal{D}}$) only for wavenumbers $k < k_{th}$ in (e) deterministic and (f) FHD simulations. (g,h) Same as (e,f), respectively, but only for wavenumbers $k > k_{th}$.

of highly intermittent behaviour, are not observed in FHD simulations. On the other hand, the skewness of velocity gradient $S^{>}(k)$ in figure 6(b) saturates to its Gaussian value, as expected, for both FHD and deterministic simulations at high k. However at low k, deterministic simulations exhibit a negative skewness with large variability, whereas it is of a much smaller magnitude and variability in FHD simulations. We note that in a recent study on the role of molecular fluctuations in incompressible turbulence (Bell et al. 2022), the skewness and kurtosis of the velocity gradient were reported to be unaffected by molecular fluctuations. Furthermore, through the analysis of structure functions in recent studies on stochastic shell modelling of incompressible turbulence (Bandak et al. 2022) and molecular gas dynamics simulations of compressible turbulence (McMullen, Torczynski & Gallis 2023), it was observed that while the fardissipation range intermittency is replaced by Gaussian fluctuations, the intermittency in the intermediate range persists. While our results are consistent with the studies in the far-dissipation range, our observations of drastically reduced intermittency in the neardissipation range can potentially be attributed to low-Re flows simulated here and/or compressibility effects.

A visual analysis of the filtered invariants of velocity gradient (i.e. vorticity magnitude $|\omega|$ and divergence \mathcal{D}) highlights our observations. Figures 7(a) and 7(b) show two-dimensional slices of vorticity magnitude $|\omega|$, and figures 7(e) and 7(f) show two-dimensional slices of divergence \mathcal{D} filtered for wavenumbers $k < k_{th}$. Similarly, figures 7(c) and 7(d), and figures 7(g) and 7(h), show the same data but filtered for wavenumbers $k > k_{th}$. While these fields 'appear' similar at large wavelengths, $k < k_{th}$, in FHD and deterministic simulations, the visual differences are significant wavenumbers $k > k_{th}$. Here, FHD simulations exhibit a nearly homogeneous spatial distribution of vorticity and divergence with no signs of intermittency, whereas deterministic simulations exhibit classic signs of dissipation-range intermittency with localised bursts of high vorticity and divergence in a 'sea' of quiescent fluid.

4. Discussion

Our simulations demonstrate that molecular fluctuations fundamentally modify compressible turbulence across the entire dissipation range, in both the energy spectrum and significantly reduced spatio-temporal intermittency. We propose that compressible fluctuating hydrodynamics (FHD) equations are a more appropriate mathematical model for compressible turbulence than the Navier–Stokes equations, especially for modelling dissipation-range physics. While FHD equations assume local thermodynamic equilibrium, they have successfully modelled compressible flows with large density gradients that compared well with molecular gas dynamics that make no such assumption (Srivastava *et al.* 2023). Importantly, even for weakly compressible turbulent flows, the present results correspond well to recent molecular gas dynamics simulations of decaying turbulence (McMullen *et al.* 2022). However, the validity of FHD in strongly compressible turbulent flows with hydrodynamic shocks remains to be established and is a significant mathematical challenge.

In principle, our predictions can be tested in experiments; however, most current experiments lack spatial and temporal resolution, and sensitivity, to accurately probe dissipation-range turbulence (Bandak *et al.* 2022). While some recent advances appear promising (van de Water *et al.* 2022), the role of molecular fluctuations in turbulence can also be indirectly evidenced in physical processes (Bandak *et al.* 2022). For example, molecular fluctuations have large observed macroscale effects in laminar diffusive mixing (Vailati & Giglio 1997) and reacting flows (Lemarchand & Nowakowski 2004); we can expect that molecular fluctuations will also impact the turbulent form of these processes. However, existing models of turbulent mixing (Sreenivasan 2019) and combustion (Sreenivasan 2004) do not account for them. Molecular fluctuations can also play an important role in transition to turbulence (Betchov 1961), and recent efforts have explored the receptivity of a compressible boundary layer to molecular fluctuations, with design implications for high-speed aircraft (Fedorov 2015; Luchini 2017).

Our results motivate new theoretical developments in turbulence closure models (Zhou 2021) that correctly account for molecular fluctuations and its impact on intermittency. Correspondingly, the latest developments in computational FHD to model thermal noise in multicomponent (Srivastava *et al.* 2023) and reactive (Polimeno *et al.* 2025) flows will facilitate a new class of direct numerical simulations that can utilise exascale supercomputers to directly investigate the role of molecular fluctuations in a variety of large-scale turbulent flows.

Supplementary material. Supplementary material is available at https://doi.org/10.1017/jfm.2025.10796.

Funding. This work was supported by the US Department of Energy (DOE), Office of Science, Office of Advanced Scientific Computing Research, Applied Mathematics Program under contract no. DE-AC02-05CH11231. This research used resources of the Oak Ridge Leadership Computing Facility at the Oak Ridge National Laboratory, which is supported by the Office of Science of the DOE under contract no. DE-AC05-00OR22725. This research also used resources of the National Energy Research Scientific Computing Center (NERSC), DOE Office of Science User Facility supported by the Office of Science of the DOE under contract no. DE-AC02-05CH11231 using NERSC award ASCR-ERCAP0026881.

Declaration of interests. The authors report no conflict of interest.

Data availability statement. The code/data that support the findings of this study are openly available in the github repository: https://github.com/AMReX-FHD/FHDeX.

Appendix. High-performance computing

The numerical method described here is implemented within the AMReX framework (Zhang *et al.* 2019), which uses an MPI paradigm for massively parallel simulations along

with GPU-based performance acceleration. The numerical method has been implemented in the fluctuating hydrodynamics software FHDeX, and it is available online as open-source code at https://github.com/AMReX-FHD/FHDeX.

Most of the simulations were performed on the exascale supercomputing platform Frontier, at the Oak Ridge National Laboratory. Each simulation run utilised either 256 or 512 compute nodes of Frontier; each compute node has 64-core AMD 'Optimized 3rd Gen EPYC' CPUs and 4 AMD Instinct MI250X GPUs, where each GPU features two Graphics Compute Dies (GCDs) for a total of eight GCDs per compute node. All the simulations were run for approximately 1.5×10^6 to 2×10^6 time steps, including the initial run to reach the steady state, followed by simulation runs to extract turbulence statistics. In total, approximately 15 000 GPU-hours were utilised to perform the simulations and analysis in this work, and $\mathcal{O}(10^2)$ terabytes of raw data were generated.

REFERENCES

- ALEXAKIS, A. & BIFERALE, L. 2018 Cascades and transitions in turbulent flows. Phys. Rep. 767, 1-101.
- ALUIE, H. 2011 Compressible turbulence: the cascade and its locality. Phys. Rev. Lett. 106 (17), 174502.
- BANDAK, D., EYINK, G.L., MAILYBAEV, A. & GOLDENFELD, N. 2021 Thermal noise competes with turbulent fluctuations below millimeter scales. arXiv preprint arXiv:2107.03184.
- BANDAK, D., GOLDENFELD, N., MAILYBAEV, A.A. & EYINK, G. 2022 Dissipation-range fluid turbulence and thermal noise. *Phys. Rev. E* **105** (6), 065113.
- BELL, J.B., NONAKA, A., GARCIA, A.L. & EYINK, GR. 2022 Thermal fluctuations in the dissipation range of homogeneous isotropic turbulence. *J. Fluid Mech.* **939**, A12.
- BENDER, J.D. 2021 Simulation and flow physics of a shocked and reshocked high-energy-density mixing layer. J. Fluid Mech. 915, A84.
- BENZI, R., BIFERALE, L., FISHER, R.T., KADANOFF, L.P., LAMB, D.Q. & TOSCHI, F. 2008 Intermittency and universality in fully developed inviscid and weakly compressible turbulent flows. *Phys. Rev. Lett.* 100 (23), 234503.
- BETCHOV, R. 1957 On the fine structure of turbulent flows. J. Fluid Mech. 3 (2), 205-216.
- BETCHOV, R. 1961 Thermal agitation and turbulence. In *Rarefied Gas Dynamics* (ed. L. Talbot), pp. 307–321. Academic Press.
- BIXON, M. & ZWANZIG, R. 1969 Boltzmann–Langevin equation and hydrodynamic fluctuations. *Phys. Rev.* **187** (1), 267–272.
- BUARIA, D. & SREENIVASAN, K.R. 2020 Dissipation range of the energy spectrum in high Reynolds number turbulence. *Phys. Rev. Fluids* **5** (9), 092601.
- CHEVILLARD, L., CASTAING, B. & LÉVÊQUE, E. 2005 On the rapid increase of intermittency in the near-dissipation range of fully developed turbulence. Eur. Phys. J. B 45 (4), 561–567.
- DE ZARATE, J.M.O. & SENGERS, J.V. 2006 Hydrodynamic Fluctuations in Fluids and Fluid Mixtures. Elsevier.
- DONEV, A., BELL, J.B., DE LA FUENTE, A. & GARCIA, A.L. 2011 Diffusive transport by thermal velocity fluctuations. *Phys. Rev. Lett.* **106** (20), 204501.
- DONEY, A., VANDEN-EIJNDEN, E., GARCIA, A. & BELL, J. 2010 On the accuracy of finite-volume schemes for fluctuating hydrodynamics. *Commun. Appl. Maths Comput. Sci.* 5, 149–197.
- DONZIS, D.A. & JOHN, J.P. 2020 Universality and scaling in homogeneous compressible turbulence. *Phys. Rev. Fluids* **5** (8), 084609.
- ESPAÑOL, P. 1998 Stochastic differential equations for non-linear hydrodynamics. *Physica A* 248 (1–2), 77–96. ESPAÑOL, P., ANERO, J.G. & ZÚÑIGA, I. 2009 Microscopic derivation of discrete hydrodynamics. *J. Chem. Phys.* 131, 244117.
- ESWARAN, V. & POPE, S.B. 1988 An examination of forcing in direct numerical simulations of turbulence. *Comput. Fluids* **16** (3), 257–278.
- EYINK, G. 2024 Onsager's 'ideal turbulence' theory. J. Fluid Mech. 988, P1.
- EYINK, G. & JAFARI, A. 2022 High Schmidt-number turbulent advection and giant concentration fluctuations. *Phys. Rev. Res.* **4** (2), 023246.
- EYINK, G.L. & DRIVAS, T.D. 2018 Cascades and dissipative anomalies in compressible fluid turbulence. *Phys. Rev. X* **8** (1), 011022.
- EYINK, G.L. & SREENIVASAN, K.R. 2006 Onsager and the theory of hydrodynamic turbulence. *Rev. Mod. Phys.* **78** (1), 87–135.

- FEDERRATH, C., KLESSEN, R.S., IAPICHINO, L. & BEATTIE, J.R. 2021 The sonic scale of interstellar turbulence. *Nat. Astron.* **5** (4), 365–371.
- FEDOROV, A.V. 2015 Prediction and control of laminar-turbulent transition in high-speed boundary-layer flows. *Proc. IUTAM* 14, 3–14.
- FORSTER, D., NELSON, D.R. & STEPHEN, M. J. 1977 Large-distance and long-time properties of a randomly stirred fluid. *Phys. Rev. A* 16 (2), 732–749.
- FOX, R.F. & UHLENBECK, G.E. 1970a Contributions to non-equilibrium thermodynamic. I. Theory of hydrodynamical fluctuations. *Phys. Fluids* 13, 1893.
- FOX, R.F. & UHLENBECK, G.E. 1970b Contributions to nonequilibrium thermodynamics. II. Fluctuation theory for the Boltzmann equation. *Phys. Fluids* 13, 2881.
- FRISCH, U. 1995 Turbulence: the Legacy of A.N. Kolmogorov. Cambridge University Press.
- FRISCH, U. & MORF, R. 1981 Intermittency in nonlinear dynamics and singularities at complex times. *Phys. Rev. A* 23 (5), 2673.
- FRISCH, U. & VERGASSOLA, M. 1991 A prediction of the multifractal model: the intermediate dissipation range. *Europhys. Lett.* **14** (5), 439.
- GARDINER, C.W. 1985 Handbook of Stochastic Methods, vol. 3. Springer.
- GARRATT, J.R. 1994 The atmospheric boundary layer. Earth-Sci. Rev. 37 (1-2), 89-134.
- GIOVANGIGLI, V. 2012 Multicomponent Flow Modeling. Birkhäuser.
- HAMLINGTON, P.E., POLUDNENKO, A.Y. & ORAN, E.S. 2012 Intermittency in premixed turbulent reacting flows. *Phys. Fluids* **24** (7), 075111.
- KHURSHID, S., DONZIS, D.A. & SREENIVASAN, K.R. 2018 Energy spectrum in the dissipation range. *Phys. Rev. Fluids* 3 (8), 082601.
- KRAICHNAN, R.H. 1967 Intermittency in the very small scales of turbulence. *Phys. Fluids* 10 (9), 2080–2082.
 LANDAU, L.D. & LIFSHITZ, E.M. 1959 *Fluid Mechanics, Course of Theoretical Physics*, vol. 6. Pergamon Press.
- LANDAU, L.D. & LIFSHITZ, E.M. 1980 Statistical Physics Part I. 3rd edn. Elsevier.
- LEMARCHAND, A. & NOWAKOWSKI, B. 2004 Fluctuation-induced and nonequilibrium-induced bifurcations in a thermochemical system. *Mol. Simul.* **30** (11–12), 773–780.
- LUCHINI, P. 2017 Receptivity to thermal noise of the boundary layer over a swept wing. AIAA J. 55 (1), 121–130.
- MAC LOW, M.-M. & KLESSEN, R.S. 2004 Control of star formation by supersonic turbulence. *Rev. Mod. Phys.* **76** (1), 125.
- McMullen, R.M., Krygier, M.C., Torczynski, J.R. & Gallis, M.A. 2022 Navier–Stokes equations do not describe the smallest scales of turbulence in gases. *Phys. Rev. Lett.* 128 (11), 114501.
- MCMULLEN, R.M., TORCZYNSKI, J.R. & GALLIS, M.A. 2023 Thermal-fluctuation effects on small-scale statistics in turbulent gas flow. *Phys. Fluids* **35** (1), 011705.
- MOROZOV, V.G. 1984 On the Langevin formalism for nonlinear and nonequilibrium hydrodynamic fluctuations. *Physica A: Stat. Mech. Applics* **126** (3), 443–460.
- VON NEUMANN, J. 1949 Recent theories of turbulence. Collected Works vol. 6. Pergamon Press. 437-472.
- PALADIN, G. & VULPIANI, A. 1987 Anomalous scaling laws in multifractal objects. *Phys. Rep.* **156** (4), 147–225.
- POLIMENO, M., KIM, C., BLANCHETTE, F., SRIVASTAVA, I., GARCIA, A.L., NONAKA, A.J. & BELL, J.B. 2025 Thermodynamic consistency and fluctuations in mesoscopic stochastic simulations of reactive gas mixtures. *J. Chem. Phys.* 162 (15), 154107.
- POPE, S.B. 2001 Turbulent Flows. IOP Publishing.
- SAGAUT, P. & CAMBON, C. 2018 Compressible homogeneous isotropic turbulence. In *Homogeneous Turbulence*, pp. 621–687. Springer International Publishing.
- SREENIVASAN, K.R. 2004 Possible effects of small-scale intermittency in turbulent reacting flows. *Flow Turbul. Combust.* **72**, 115–131.
- SREENIVASAN, K.R. 2019 Turbulent mixing: a perspective. *Proc. Natl Acad. Sci. USA* 116 (37), 18175–18183.
- SRIVASTAVA, I., LADIGES, D.R., NONAKA, A.J., GARCIA, A.L. & BELL, J.B. 2023 Staggered scheme for the compressible fluctuating hydrodynamics of multispecies fluid mixtures. *Phys. Rev. E* **107** (1), 015305.
- TREMBLAY, A.-M.S., ARAI, M. & SIGGIA, E.D. 1981 Fluctuations about simple nonequilibrium steady states. *Phys. Rev. A* 23 (3), 1451.
- URZAY, J. 2018 Supersonic combustion in air-breathing propulsion systems for hypersonic flight. Annu. Rev. Fluid Mech. 50 (1), 593–627.
- USABIAGA, F.B., BELL, J.B., DELGADO-BUSCALIONI, R., DONEV, A., FAI, T.G., GRIFFITH, B.E. & PESKIN, C.S. 2012 Staggered schemes for fluctuating hydrodynamics. *Multiscale Model. Simul.* 10 (4), 1369–1408.
- VAILATI, A. & GIGLIO, M. 1997 Giant fluctuations in a free diffusion process. *Nature* 390 (6657), 262–265.

- WANG, J., GOTOH, T. & WATANABE, T. 2017 Scaling and intermittency in compressible isotropic turbulence. *Phys. Rev. Fluids* **2** (5), 053401.
- WANG, J., SHI, Y., WANG, L.-P., XIAO, Z., HE, X.T. & CHEN, S. 2012 Scaling and statistics in three-dimensional compressible turbulence. *Phys. Rev. Lett.* **108** (21), 214505.
- WANG, J., YANG, Y., SHI, Y., XIAO, Z., HE, X.T. & CHEN, S. 2013 Cascade of kinetic energy in three-dimensional compressible turbulence. *Phys. Rev. Lett.* **110** (21), 214505.
- VAN DE WATER, W., DAM, N. & CALZAVARINI, E. 2022 Dispersion of molecular patterns written in turbulent air. *Phys. Rev. Lett.* **129** (25), 254501.
- Wu, M., Ahlers, G. & Cannell, D.S. 1995 Thermally induced fluctuations below the onset of Rayleigh–Bénard convection. *Phys. Rev. Lett.* **75** (9), 1743–1746.
- YEUNG, P.K., ZHAI, X.M. & SREENIVASAN, K.R. 2015 Extreme events in computational turbulence. *Proc. Natl Acad. Sci. USA* 112 (41), 12633–12638.
- ZHANG, W. 2019 AMReX: a framework for block-structured adaptive mesh refinement. J. Open Sour. Softw. 4 (37), 1370.
- ZHOU, Y. 2021 Turbulence theories and statistical closure approaches. Phys. Rep. 935, 1–117.
- ZUBAREV, D.N. & MOROZOV, V.G. 1983 Statistical mechanics of nonlinear hydrodynamic fluctuations. Physica A 120 (3), 411–467.